



Biosynthesis of NiO Nanoparticles Using Soursop (*Annona muricata* L.) Fruit Peel Green Waste and Their Photocatalytic Performance on Crystal Violet Dye

Mohammad Aminuzzaman¹ · Chan-Yong Chong¹ · Wee-Sheng Goh¹ · You-Kang Phang¹ · Tey Lai-Hock¹ · Swee-Yong Chee¹ · Md. Akhtaruzzaman² · Sayaka Ogawa³ · Akira Watanabe³

Received: 1 June 2020 / Published online: 17 August 2020
© Springer Science+Business Media, LLC, part of Springer Nature 2020

Abstract

A simple, inexpensive, and eco-friendly route has been demonstrated for synthesizing spherical NiO nanoparticles (NiO NPs) with a size range between 20 and 90 nm using aqueous extract of soursop (*Annona muricata* L.) fruit peel green waste which plays the role of reducing and stabilizing agent during the synthesis. The formation, morphology, structure and other physicochemical properties of the resulting NiO NPs were characterized by various experimental techniques such as X-ray diffraction (XRD), energy dispersive X-ray (EDX) analysis, Raman spectroscopy, X-ray photoelectron spectroscopy (XPS), ultraviolet–visible (UV–vis) spectroscopy, Fourier transform infrared (FT-IR) spectroscopy, field emission scanning electron microscopy (FESEM) and transmission electron microscopy (TEM). The photocatalytic performance of the prepared NiO NPs was assessed toward the photodegradation of crystal violet (CV) dye as a model pollutant under sunlight illumination. The measurement of chemical oxygen demand (COD) values verified the degree mineralization of CV dye. The results show that nearly 99.0% of CV pollutant was photodegraded at 105 min of illumination, making it a promising candidate for wastewater treatment.

Keywords Green synthesis · NiO nanoparticles · Green waste · Photocatalyst · Photodegradation

Electronic supplementary material The online version of this article (<https://doi.org/10.1007/s10876-020-01859-8>) contains supplementary material, which is available to authorized users.

✉ Mohammad Aminuzzaman
mohammoda@utar.edu.my

¹ Department of Chemical Science, Faculty of Science, Universiti Tunku Abdul Rahman (UTAR), Perak Campus, Jalan Universiti, Bnadar Barat, 31900 Kampar, Perak D. R., Malaysia

² Solar Energy Research Institute (SERI), Universiti Kebangsaan Malaysia (UKM), 43600 Bangi, Selangor, Malaysia

³ Institute of Multidisciplinary Research for Advanced Materials (IMRAM), Tohoku University, Katahira 2-1-1, Aoba-ku, Sendai 980-8577, Japan

Introduction

Pollution of water resources by anthropogenic pollutants such as organic dyes, pigments, heavy metals, herbicides, and antibiotics is a growing environmental disquietude. Among various water pollutants, organic dyes cause a significant threat for all living beings, ranging from aquatic species to human beings even at low concentrations [1]. Moreover, many of the organic dyes along with their products are carcinogenic and mutagenic in nature responsible for number sorts of cancers for human beings [2–4]. Consequently, it is a matter of great concern to treat these dyes before releasing into water resources. In the recent past, various physico-chemical methods have been developed to eliminate these toxic organic dyes from industry effluent/wastewater to decrease their environmental impact. These methods include biological methods (aerobic and anaerobic processes) [5], adsorption [6–8], chemical oxidation [9], ion exchange [10], coagulation–flocculation [11–13], photocatalytic degradation [14, 15], electrochemical processes [16], membrane filtration [17],

precipitation [18], and reverse osmosis [19]. Among them, semiconductor photocatalysis has drawn huge attention for degrading organic dyes in wastewater by exploiting the energy from natural sunlight or artificial illumination due to its relatively safe reaction conditions, low cost, high degradation efficiency, broad applied area, and easy manipulation. The principle of photocatalytic reaction is based on the absorption of photons by the semiconductor photocatalyst consequences in promoting of an electron from the valence band to conduction band, thus creating an electron deficiency or hole (h^+) in the valence band and concurrently generating an electron (e^-) in the conduction band. The produced e^-/h^+ pairs move towards the surface of the semiconductor photocatalyst and undergo redox reactions to generate reactive species such as hydroxyl ($\cdot OH$) radicals which then ultimately degrade the hazardous organic dye pollutants into environmentally benign species like H_2O , CO_2 , NO_2 , NO etc. Nanostructured semiconductor metal oxides have become the attractive photocatalyst for organic pollutants degradation in aqueous media owing to their easy availability, nontoxicity, and biological and chemical stability. Among those nanostructured semiconductor metal oxides, nickel oxide (NiO) is a p -type semiconductor with a wide band gap ranging from 3.6 to 4.0 eV, making it specifically suitable as photocatalyst [20]. The photocatalytic efficiency of NiO is influenced by various factors such as band gap energy (E_g), crystallinity, surface area, and particle size etc. Several strategies such as solvothermal [21], sol-gel [22, 23], sonochemical [24], chemical precipitation [25], microemulsion [26], spray pyrolysis [27], microwave synthesis [28–30], hydrothermal [31], thermal decomposition [32], anodic arc plasma method [33] etc. have been stated to achieve NiO nanomaterials in varied morphologies. However, most of these strategies are associated with several disadvantages including utilization of hazardous organic solvents, toxic chemicals as reducing agents and sophisticated equipments, low yield, wearisome procedures, and rigorous experimental conditions along with high operational cost. With increasing concerns over environmental pollution, researchers are putting in lot of efforts in developing green synthesis protocols for the fabrication NiO nanoparticles (NiO NPs) using innocuous, eco-friendly, and renewable materials such as those evolved from natural sources including plants, bacteria, yeast, fungi and microalgae. Plants are regarded to be the most viable candidate in terms of simplicity, better reducing efficiency, easier availability and high content of vast range of bioactive molecules. Phytochemicals such as polyphenols, terpenoids, flavonoids, alkaloids, sugars, proteins etc. with wide range of reductive capacities in plant extracts play a crucial role in controlling the morphology, size, and yield of nanoparticles during synthesis. Moreover, plant extracts mediated

synthesized nanoparticles have better stability, biocompatibility and biosafety than those obtained from chemical synthesis. The green synthesis of NiO NPs from the plant extract including *Moringa oleifera* (leaf) [34], *Agathosma betulina* (leaf) [35], *Aegele marmelos* (leaf) [36], *Aspalathus linearis* (leaf) [37], *Calotropis gigantea* (leaf) [38], *Monsonia burkenia* (leaf) [39], *Ananas comosus* (leaf) [40], *Euphorbia heterophylla* (leaf) [41], *Tamarix serotina* (flower) [42], *Hydrangea paniculata* (flower) [43], and *Nephelium lappaceum* (fruit peel) [44] have been reported in the literature.

Annona muricata (L.) (*A. muricata*) which is commonly known as soursop belongs to the family of *Annonaceae*. *A. muricata* is a small, upright evergreen tree, about 5–8 m in height with large, dark green leaves and is mostly found in tropical and subtropical regions of the world. The edible fruits of the tree are large, oval or heart-shaped and light green in color when fully ripe with a white fibrous flesh. Traditionally, various parts (bark, root, leaf, seed, and fruit) of *A. muricata* have been used as medicine to treat arthritic pain, neuralgia, respiratory illness, diarrhea, dysentery, fever, malaria, and cancer especially liver and breast [45]. Phytochemical studies reveals that different parts of *A. muricata* plant contain secondary metabolites such as acetogenins, alkaloids, phenols, flavonoids, carbohydrates, terpenoids and proteins [46–48]. These phytochemicals may act as reducing agent as well as capping agent in the synthesis of nanoparticles. The present study focuses, the synthesis and characterization of NiO NPs using nickel acetate as precursor and aqueous extract of *A. muricata* fruit peel. Furthermore, photocatalytic performance of NiO NPs was evaluated by photodegradation of crystal violet dye utilizing the naturally abundant solar irradiation.

Materials and Methods

Materials

Fresh soursop fruits had been obtained from a neighborhood market in the state of Perak at Kampar in Malaysia. All the chemicals had been in analytical grade and used as-purchased without further purification. $Ni(CH_3COO)_2 \cdot 2H_2O$ and crystal violet dye (CV) dye were obtained from Sigma-Aldrich, USA. All aqueous solutions were prepared using deionized water.

Preparation of the extract

Fresh peels of soursop were washed utterly with water to eliminate dirt and subsequently cut into small pieces. 100 g of peels were taken in a 250 ml beaker with 100 ml deionized water and heated for 30 min at 80 °C. Upon

cooling, the peel extract was filtered through vacuum filtration and the pale yellow filtrate was collected in a 100 ml beaker. In the synthesis of NiO NPs this freshly prepared extract is directly used. In order to screen the phytochemicals, the peel extract was subjected to various chemical tests according to standard procedures [49, 50].

Synthesis of NiO NPs

Scheme 1 shows the synthesis process of NiO NPs. At first, the freshly prepared 50 ml soursop fruit peel extract was heated at 70–80 °C in a 100 ml beaker. Subsequently about 2 g of $\text{Ni}(\text{CH}_3\text{COO})_2 \cdot 2\text{H}_2\text{O}$ was added slowly into the hot extract. This mixture was heated at about 70 °C with continuous stirring. The color of the reaction solution gradually changed from light green to dark green as the reaction progressed and heating was continued until the formation of a dark green color paste as shown in Scheme 1. On subsequent cooling, the dark green colored paste was washed vigorously with deionized water followed by ethanol. Finally, the paste was vacuum-dried at 100 °C for 30 min. Afterward, the paste was calcinated at 450 °C for 2.5 h in a temperature controlled muffle furnace (air ambient). The resultant black colored product was used for characterization using various analytical techniques.

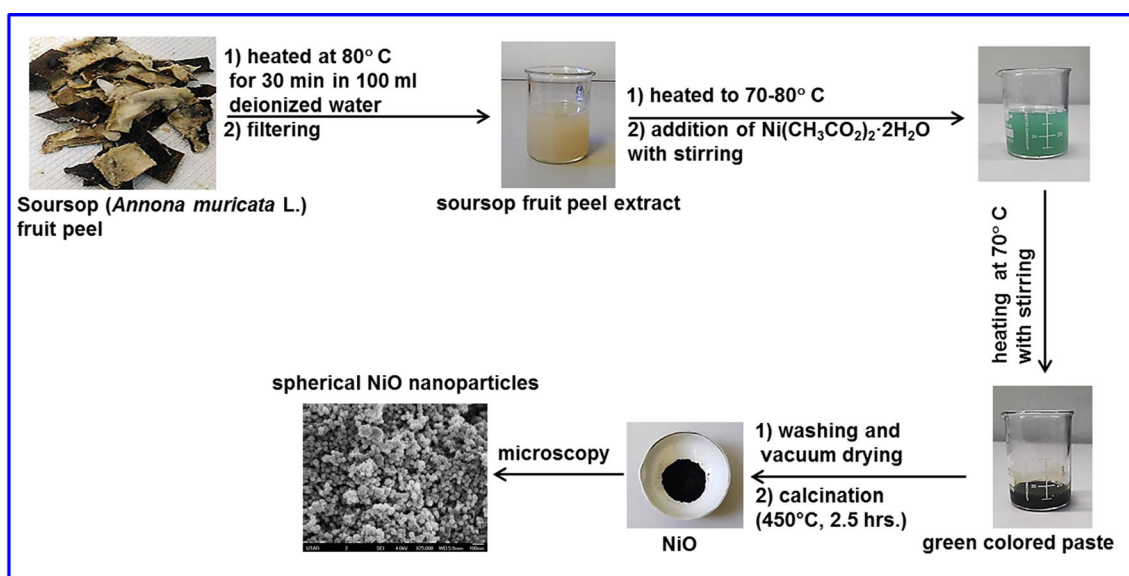
Characterization of NiO NPs

A Shimadzu XRD 6000 X-ray diffractometer (operating at a voltage of 40 kV and 40 mA with $\text{CuK}\alpha$ radiation of 1.5418 Å in the 2θ range of 10°–90°) was used to study the crystal structure of NiO. A field emission scanning electron microscopy (FESEM, JEOL JSM-6701F, Japan coupled

with EDX, X-max 150, Oxford Instruments) and a high resolution transmission electron microscopy (HRTEM) (JEOL JEM-3010) were performed to describe the morphological and microstructural details of NiO NPs. UV–vis absorption spectra were measured by GENESYS 180 (Thermo Scientific) UV–vis spectrophotometer. A Perkin-Elmer RX1 FTIR spectrophotometer was used to investigate the structural identity of NiO. FTIR measurements were carried out in the transmittance mode in the spectral range of 400–4000 cm^{-1} with the resolution of 4 cm^{-1} by the KBr pellet method. The X-ray photoelectron spectra were obtained using an ESCA 5300 X-ray photoelectron spectrometer (XPS) (Parkin-Elmer) with $\text{MgK}\alpha$ X-ray as the excitation source. Raman spectrum was measured on a micro-Raman spectrometer equipped with an optical microscope (Olympus BX51), a CW 532 nm DPSS laser, a peltier-cooled CCD camera (DV401, Andor Technology), and a monochromator (MS257, Oriel Instruments Co.).

Photocatalytic Performance of NiO NPs

The photocatalytic performance of the as-prepared NiO NPs was examined by the photodegradation of an aqueous solution of crystal violet (CV) dye under the illumination of sunlight in an open atmosphere. The photocatalytic experiments of CV dye was accomplished on the days of bright sunny light in between 10 am to 2 pm in the Kampar campus of Universiti Tunku Abdul Rahman (UTAR) with an average solar radiation was of 4.30 $\text{kW h m}^{-2} \text{day}^{-1}$. In a typical procedure, 50 mg of the catalyst was dispersed in a CV dye aqueous solution (50 mL, 20 mg/L) under ultrasonication for 5 min. Prior to the illumination, the reaction suspension was stirred for 1 h in the dark to attain



Scheme 1 Diagrammatic Illustration for Green Synthesis of NiO Nanoparticles

adsorption–desorption equilibrium between CV dye and the photocatalyst. The suspension was then exposed to sunlight irradiation while being stirred continuously. 10 mL of the suspension was periodically collected and centrifuged (Eppendorf Centrifuge 5702, 7000 rpm, 30 min) to remove the remnant NiO NPs. A UV–vis spectrophotometer was used to measure the concentration of CV dye in the supernatant. The percentage of CV dye degradation has been calculated using the following equation (1):

$$\text{Dye degradation(\%)} = \frac{C_0 - C_t}{C_0} \times 100 \quad (1)$$

where C_0 and C_t are the initial and remaining concentrations of CV dye at different times, respectively.

The Chemical Oxygen Demand (COD) of CV dye solution before and after the photocatalytic degradation process were measured using a low range COD (HACH 21258 vial digestion solution COD-LR) vial from Hach Company, Germany. A 2 mL of CV dye solution (or photodegraded parts) was added into the COD-LR vial which was then subjected to a digestion process at 150 °C for 2 h using a HACH DRB 200 COD digital reactor. After that, the COD values of CV dye and photodegraded parts (mg/L) were determined using a DR-6000 UV–vis spectrophotometer (Hach, Germany).

Results and Discussion

Structural Analysis of NiO NPs

The X-ray diffraction (XRD) pattern (Fig. S1) (Supplementary information) revealed the overall crystal structure and phase purity of the synthesized NiO NPs. The diffraction peaks of spherical NiO NPs are indexed as cubic phase and well-matched with International Centre for Diffraction Data (ICDD): Entry number-01-071-6723. The observed diffraction patterns of NiO NPs had been located at $2\theta = 37.24^\circ$, 43.32° , 62.80° , 75.64° , and 79.50° are corresponding to reflection planes of (111), (200), (220), (311), and (222), respectively. The sharp and high intensity of the diffraction peaks of NiO NPs genuinely implied the high crystallinity. It was observed that the (200) reflection of plane was the preferred orientation and the NiO NPs were grown in the (200) direction. The crystallite size (D) of the NiO was calculated from the high intense diffraction peak (200) using Debye–Scherrer's equation (2):

$$D = \frac{0.94\lambda}{\beta \cos\theta} \quad (2)$$

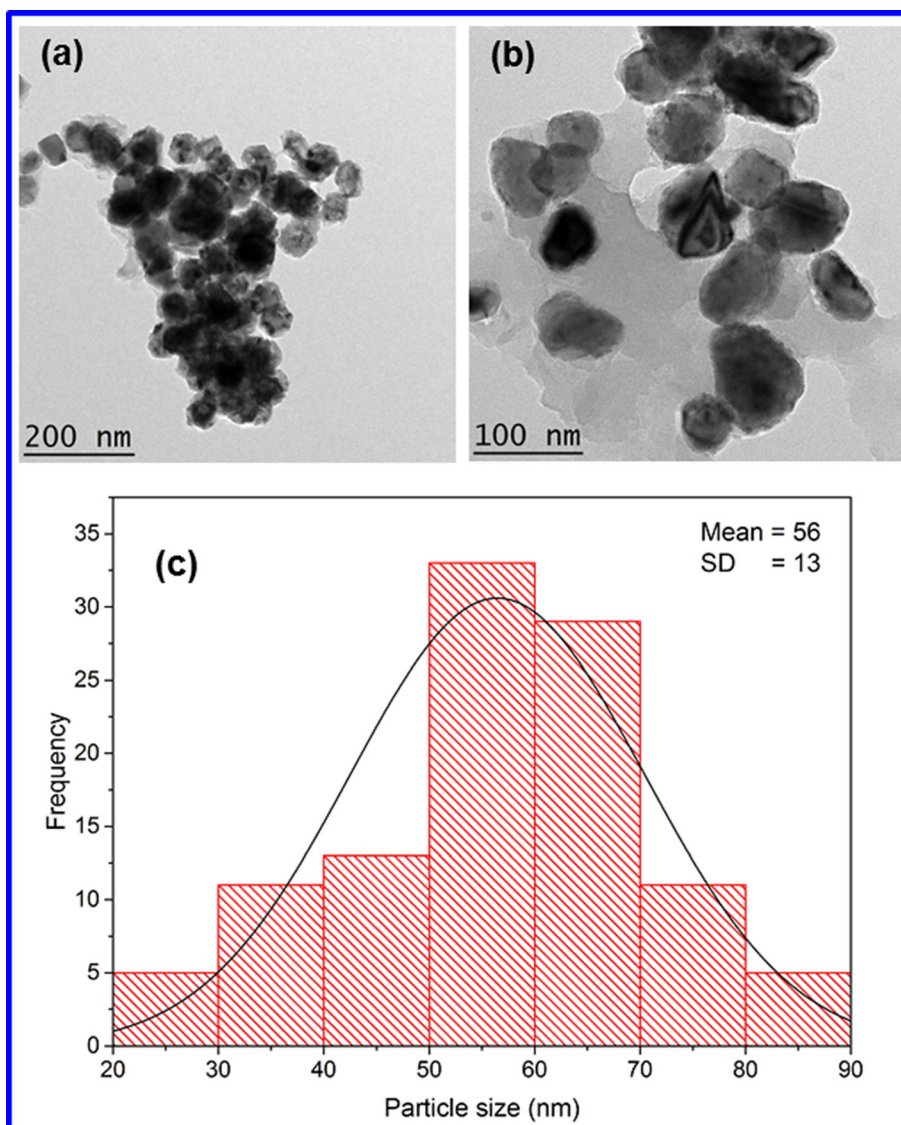
where λ is the wavelength of X-ray (1.5418 Å) for $\text{CuK}\alpha$ radiation, β is the full width half maximum (FWHM) of the

prominent intense peak (using the 100% relative intensity peak were used) and θ is the peak position. The crystallite size of NiO NPs was found to be 50.50 nm. However, before calcination the dark green paste did not show any sharp diffraction peaks of NiO but showed a broad peak located at $2\theta = 24.0^\circ$ with a low intensity suggesting amorphous phase of the dark green paste. For further confirmation of NiO NPs, Raman spectrum was observed in the range of 90 cm^{-1} to 1800 cm^{-1} as shown in Fig. S2 (Supplementary information). The Raman spectrum showed four peaks at around 400, 520, 700, and 1070 cm^{-1} , which are characteristics Raman bands reported for NiO nanomaterials [51–53]. The peaks at around 400 and 520 cm^{-1} can be assigned to the first order transverse optical (TO) and longitudinal optical (LO) phonon modes of NiO, respectively. The peaks at around 700 and 1070 cm^{-1} can be attributable to the 2TO and 2LO phonon modes, respectively.

XPS is a surface-sensitive probe that can provide valuable information on the surface composition precisely and also allow to differentiate distinctive local atomic environments i.e., the valence state and coordination of an element. Figure S3 (Supplementary information) represents XPS spectra of Ni and O regions of NiO nanoparticles. The Ni region of NiO (Fig. S3a) showed two prominent peaks located at 855.2 and 873.6 eV, assigned to Ni $2p_{3/2}$ and Ni $2p_{1/2}$, respectively and are attributed to Ni^{2+} state in NiO [54, 55]. Moreover, the peak at 860.8 eV corresponded to the satellite peak of Ni $2p_{3/2}$ while the peak at 880.0 eV is assigned to the satellite peak of Ni $2p_{1/2}$ [56]. Besides, as shown in Fig. S3b, the peak observed at 530.0 eV could be attributed to the binding energy of O 1s, which is ascribed to the O^{2-} in the NiO [57]. All these results clearly confirmed the formation of NiO as a pure product resulting from the bioreduction of $\text{Ni}(\text{CH}_3\text{COO})_2 \cdot 2\text{H}_2\text{O}$ precursor and proved the high potentiality of suorsoup fruit peel extract for the synthesis of nanomaterials. Furthermore, the purity of the NiO NPs was confirmed by energy dispersive X-ray analysis (EDX) (Fig. S4) (Supplementary information). The EDX spectrum displays Ni and O peaks and indicated the presence of NiO phase without any other impurity that is in excellent agreement with the finding XRD result. EDX analysis also provided the content of Ni and O as atomic percentage and found to be 44.73 and 55.27, respectively. The atomic ratio of Ni and O is found to be 0.81.

The electron microscopic observations for detailed morphological and size analysis of the synthesized NiO NPs are represented in Fig. 1 and Fig. S5 (Supplementary information). The TEM images showed and confirmed that as-synthesized NiO NPs are spherical in shape (Fig. 1a, b) with sizes in the range of 20–90 nm and the average size of 56 nm (Fig. 1c). The TEM images showed that particle

Fig. 1 TEM images of biosynthesized NiO NPs at different magnifications and histogram of the distribution of the particles size of NiO NPs



size ranges were in agreement with the crystallite size obtained from the XRD result. Figure S5 shows the FESEM images of NiO NPs which also showed that NiO particles are spherical in shape, in agreement with TEM micrographs and agglomerated. This agglomeration of these particles was ascribed to the magnetic interactions between the particles [34].

Figure 2 shows the UV–vis absorption spectrum of the as-synthesized NiO NPs which was measured at room temperature. The NiO NPs with the concentration of 0.1 wt% in water were ultrasonically dispersed and the resulting colloidal suspension was used to perform the UV–vis measurement. The UV–vis spectrum showed a strong absorption band located at 310 nm which can be attributed to the intrinsic band gap absorption of NiO NPs. The band gap energy was calculated according to the Tauc relationship (3):

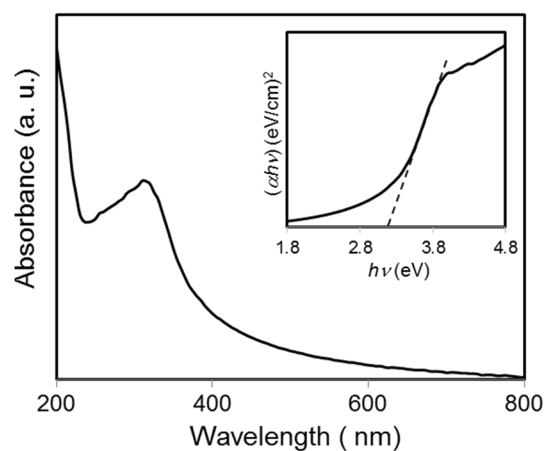


Fig. 2 UV–vis spectrum of biosynthesized NiO NPs at room temperature. The inset shows the plot of the $(\alpha h\nu)^2$ vs $(h\nu)$

$$\alpha hv = A(hv - E_g)^n \quad (3)$$

where α is the absorption coefficient, hv is the energy of a photon, A is a proportionality constant, E_g represents the optical band gap, and n is the parameter of specific electronic transition within the band due to the light absorption ($n = 1/2$ or 2 for indirect or direct transition, respectively) [58, 59]. Therefore by plotting $(\alpha hv)^2$ versus (hv) and extrapolating the linear portion of the curve to meet the energy axis (hv) E_g can be estimated which is shown in the inset of Fig. 2. In this study, the E_g value of the NiO NPs is found to be 3.22 eV. The E_g of the bulk NiO is 4.0 eV, however in this study synthesized NiO NPs exhibited decrease in E_g . Generally, semiconductor nanomaterials exhibit a blue shift in E_g due to the quantum confinement effects but a red shift was observed in our green-synthesized NiO which could be ascribed to chemical defects or vacancies nearby intergranular regions, creating new energy levels ensuing in reduction of E_g [60–62]. No linear relation was observed in Tauc plot for $n = 1/2$, indicating that our green-synthesized NiO NPs are semiconductor with direct transition at this energy state [63].

Phytochemical screening reveals the presence of tannins, alkaloids, carbohydrates, triterpenoids, steroids and flavonoids in the aqueous extract of soursop fruit peel. The potential functional groups of phytochemicals in soursop fruit peel extract that are responsible for bioreduction leading to the formation of NiO NPs was confirmed by FTIR measurements. Figure S6a (Supplementary information) represents the FTIR spectrum of soursop fruit peel extract and can be seen that the strong absorption peaks observed at 3433, 2973, 1643, and 1063 cm^{-1} can be assigned to O–H stretch, C–H stretch (alkanes), N–H bending, and C–O–C stretch, respectively. Weaker bands located at 1400, 1232, 895, and 773 cm^{-1} can be assigned to C–C stretching of aromatic ring, C=O vibration, C–O stretching, and C–H aromatics, respectively. Figure S6b (Supplementary information) shows the FTIR spectra of the dark green paste calcinated at different temperatures for 2.5 h. When the calcination temperatures were 150 °C and 300 °C for 2.5 h, there was no peak of Ni–O vibration but showed the various peaks of the biomolecules in soursop fruit peel. On the other hand, when the dark green paste was calcinated at 450 °C for 2.5 h displayed a sharp and intense peak located at 432 cm^{-1} which is attributed to Ni–O vibration in stretching mode while the absorption band observed at 3406 cm^{-1} owing to O–H stretching surface adsorbed water molecules [64]. The formation of NiO NPs could possibly attribute to the presence of phytochemicals (acetogenins, alkaloids, polyphenols, carbohydrates etc.) in soursop fruit peel which act as reducing agents as well as stabilizing agents during synthesis. Table 1 summarizes a

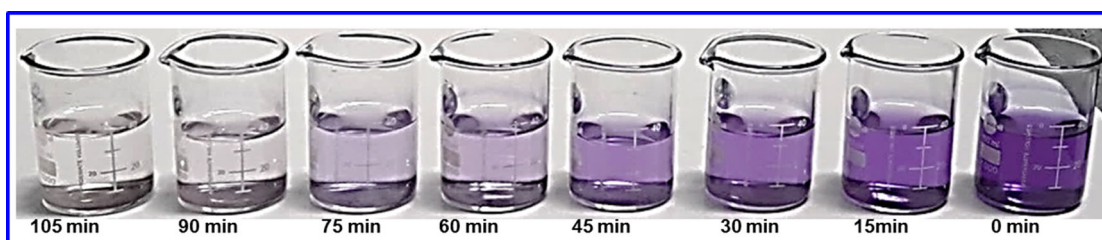
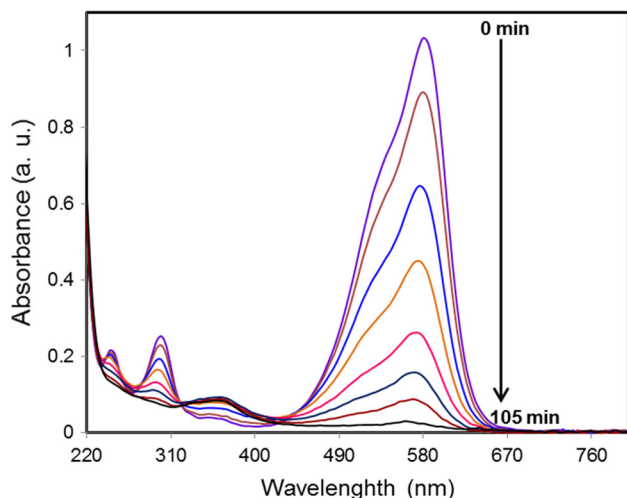
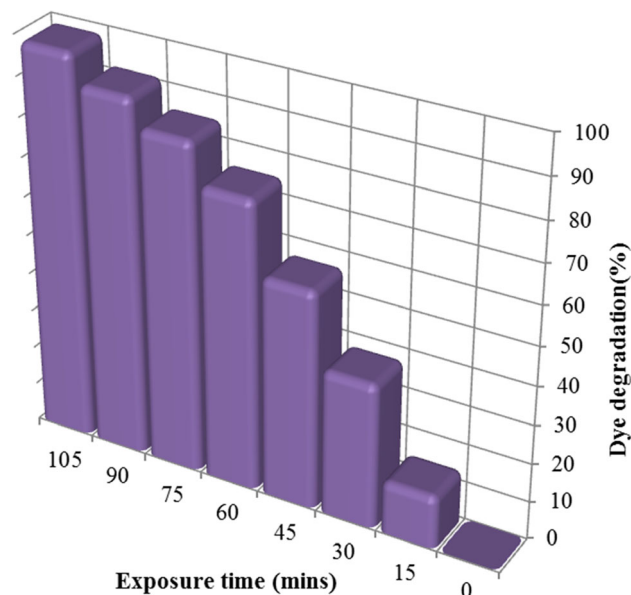
comparison of our green-synthesized NiO NPs with those reported in the literatures [35–37, 39, 43, 65, 66].

Photocatalytic Performance of Green-Synthesized NiO NPs

The photocatalytic performance of as-synthesized NiO NPs was evaluated towards the degradation of crystal violet (CV) dye solution under sunlight irradiation. CV, a synthetic triphenyl methane dye, is vastly used for various applications such as for dyeing in textile industry, manufacture of paints and printing inks as well as biological staining, dermatological agent, veterinary medicine, additive to poultry feed to inhibit propagation of mold, intestinal parasites and fungus etc. [67]. Despite extensive applications of CV, this dye poses environmental and health hazard as it is a mutagen, mitotic poison and potent carcinogenic agent due to the complex aromatic ring structure [68, 69]. The consumption of this dye even in small quantity (< 1 ppm) may cause serious effects on human health like breathing disorders, renal failure, permanent blindness etc. [70, 71]. The long conjugated heteropoly aromatic linkage in CV acts as a chromophoric group and produced strong violet color when dissolved in water. During the direct sunlight irradiation in the presence of NiO NPs, the strong violet color of CV dye solution was gradually faded and become colorless as shown in Fig. 3. This result indicates the destruction of chromophoric group and photodecomposition of CV dye. This is further confirmed by UV–vis measurements of CV solution at different solar irradiation time as shown in Fig. 4. The UV–vis spectrum of the CV solution before illumination with solar light shown characteristic prominent peaks located at 580, 300, and 230 nm that corresponding to conjugated triphenylmethane chromophore, diphenyl methyl type, $\phi_2C = (\phi, -C_6H_5)$, and benzene moieties, respectively. The results show that CV dye having the strong absorption maxima at 580 nm was diminished progressively as solar irradiation time increases from 0 min to 105 min and eventually attains nearly 99.0% of degradation efficiency. This clearly suggests cleavage of the whole conjugated chromophore structure of CV dye. With increasing solar irradiation time, the maximum absorption wavelength also shifted from 580 nm to 570 nm resulting from *N*-demethylation of the chromophore skeleton [72]. Figure 5 shows the degradation efficiency of CV dye as a function of exposure time. It demonstrates that after 105 min of exposure nearly 99% of CV was photodegraded under solar irradiation because of efficient oxidation through highly reactive hydroxyl radicals ($\cdot\text{OH}$) generated from the photocatalytic reaction. The detailed mechanism for the photodegradation of CV dye was illustrated in Scheme 2. The photodecolorization efficiency of CV dye using NiO NPs at

Table 1 A Comparison of soursop (*A. muricata* L.) fruit peel extract synthesized NiO NPs with other biosynthesized NiO NPs reported in the literatures

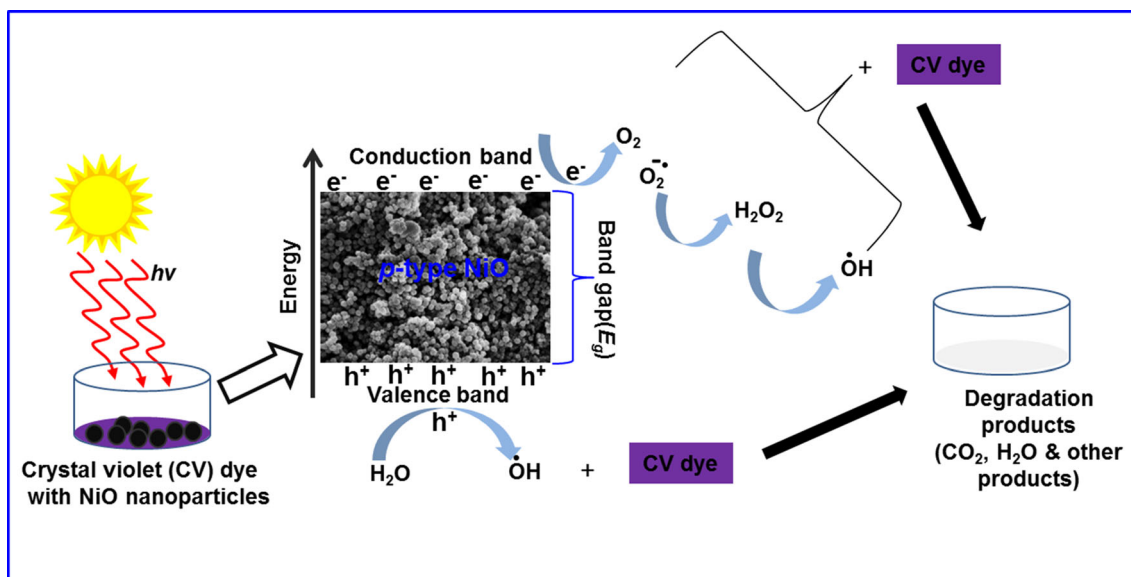
Precursor	Plant	Size of NiO NPs (nm)	Shape of NiO NPs	References
$\text{Ni}(\text{NO}_3)_2 \cdot 6\text{H}_2\text{O}$	<i>Agathosma betulina</i> (leaf)	27	Quasi-spherical	[35]
$\text{Ni}(\text{NO}_3)_2 \cdot 6\text{H}_2\text{O}$	<i>Aegle marmelos</i> (leaf)	8–10	Cubic and spherical	[36]
$\text{Ni}(\text{NO}_3)_2 \cdot 6\text{H}_2\text{O}$	<i>Aspalathus linearis</i> (leaf)	14	Quasi-spherical	[37]
$\text{Ni}(\text{NO}_3)_2 \cdot 6\text{H}_2\text{O}$	<i>Monsonia burkena</i> (leaf)	25	Mostly spherical with varied shapes	[39]
$\text{Ni}(\text{NO}_3)_2 \cdot 6\text{H}_2\text{O}$	<i>Hydrangea paniculata</i> (flower)	33	Spherical, oval and rod	[43]
$\text{Ni}(\text{NO}_3)_2 \cdot 6\text{H}_2\text{O}$	<i>Persea americana</i> (seed)	11	Spherical and rhombohedra	[65]
$\text{Ni}(\text{NO}_3)_2 \cdot 6\text{H}_2\text{O}$	<i>Terminalia chebula</i> (fruit)	20–25	Cubic	[66]
$\text{Ni}(\text{CH}_3\text{COO})_2 \cdot 2\text{H}_2\text{O}$	<i>Annona muricata</i> (fruit peel)	52	Spherical	Present work

**Fig. 3** Photograph showing gradual change in CV dye color from deep violet to colorless by solar irradiation**Fig. 4** UV-vis absorption spectra of solar photocatalytic degradation of CV dye with reaction time**Fig. 5** Degradation efficiency of CV dye solution under sunlight illumination

various reaction conditions were presented in Table 2. NiO NPs had successfully degraded CV dye molecules and forming harmless end products like CO_2 , H_2O , and other small molecules.

In order to confirm the mineralization of CV dye by NiO NPs photocatalyst, the change in COD values at different time interval of the illuminated CV solution under sunlight was measured (Fig. 6). The initial COD value for CV solution was 31.5 mg/mL and the COD values decreased

gradually as the illumination time increased, reaching 6.2 mg/mL after 105 min of exposure to sunlight. These results confirmed the high potency of green-synthesized NiO NPs as a photocatalyst for degradation of CV dye under solar irradiation. Degradation of CV dye solution carried out using green-synthesized NiO NPs has been



Scheme 2 The Schematic Pictorial Representation for the Degradation of CV Dye using green-synthesized NiO NPs

Table 2 The photodegradation efficiency of CV dye solutions using green-synthesized NiO NPs obtained from different reaction conditions

Sample	Source of light	Pollutant	Decolorization efficiency			Time
			Blank	Dark	Photocatalysis	
NiO NPs	Sunlight	Crystal violet (CV)	4%	10%	99%	105 min

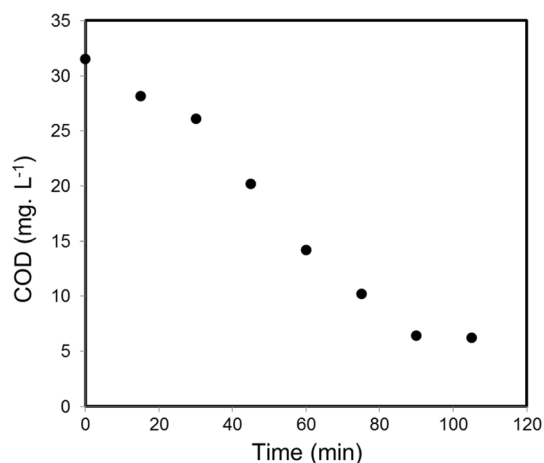


Fig. 6 Change in COD (mg L^{-1}) values of CV dye solution as a function of solar irradiation time

compared with other reported nanomaterials in literature as shown in Table 3. The comparison data reveals that photocatalytic performance of our green-synthesized NiO NPs is superior to those reported in the literatures [73–80].

Conclusions

In this study, by using the green chemistry approach, NiO NPs were successfully synthesized from nickel acetate as precursor and aqueous extract of soursop (*A. muricata* L.) fruit peel green waste as novel reducing and stabilizing agent. This low cost green technology could be potentially used for the bulk synthesis of NiO NPs for wide range of applications. The purity, crystallinity, morphology, structural features and the chemical composition of the as-prepared NiO NPs were investigated by various analytical techniques. The detailed characterization corroborates that NiO NPs are pure, highly crystalline, and having spherical shape with an average size of 56 nm. This green-synthesized NiO NPs were investigated for their performance as a photocatalyst through photocatalytic degradation of CV dye pollutant under solar irradiation. Almost 99% of degradation of CV dye was observed with 105 min of sunlight exposure and the dye was subsequently mineralized into innocuous end products. These investigations clearly demonstrate that green-synthesized NiO NPs can be used as a potential photocatalyst for the removal of hazardous pollutants present in wastewater.

Table 3 A Comparison of photocatalytic performance of biosynthesized NiO NPs with other nanomaterials on the degradation of crystal violet (CV) dye

Photocatalyst used	Synthesizing method	Concentration of CV dye (mg/L)	Catalyst dosage (mg)	Irradiation source	Degradation time (min)	Degradation efficiency (%)	References
Mn doped and PVP capped ZnO NPs	Chemically synthesized	10	250	UV light	180	100	[73]
TG capped ZnS NPs	Chemically synthesized	10	250	UV-vis light	180	96	[74]
Fe ₃ O ₄ /SnO ₂ NCs	Chemically synthesized	10	500	UV light	180	83	[75]
HgO NPs	Chemically synthesized	20	100	UV light	180	100	[76]
Cu doped ZnO NPs	Chemically synthesized	10	250	UV-vis light	210	96	[77]
F-TiO ₂ (B)/fullerene NCs	Chemically synthesized	30	10	Visible light	120	77	[78]
rGO-TiO ₂ /Co ₃ O ₄ NCs	Biologically synthesized	10	50	Visible light	120	80	[79]
FeO NPs	Biologically synthesized	10	–	Sunlight	150	80	[80]
NiO NPs	Biologically synthesized	20	50	Sunlight	105	99	Present work

Acknowledgements The authors would like to express their gratitude to Universiti Tunku Abdul Rahman (UTAR) for financial support and also for providing a conducive environment to execute this research work successfully. This work was also partially supported by JSPS KAKENHI Grant Number JP15H04132 and JSPS KAKENHI Grant Number JP19H05356. The authors also extend their appreciation to the University Research Grant at Universiti Kebangsaan Malaysia (UKM) for supporting this work through research group no. (GUP-2018-130).

References

- R. Mallampati, L. Xuanjun, A. Adin, and S. Valiyaveetil (2015). *ACS Sustainable Chem. Eng.* **3**, 1117.
- M. A. M. Salleh, D. K. Mahmoud, W. A. Karim, and A. Idris (2011). *Desalination* **280**, 1.
- W. Jiang, Y. Zhu, G. Zhu, Z. Zhang, X. Chen, and W. Yao (2017). *J. Mater. Chem. A* **5**, 5661.
- M. H. Wu, L. Li, Y. C. Xue, G. Xu, L. Tang, N. Liu, and W. Huang (2018). *Appl. Catal. B* **228**, 103.
- S. Sekar, M. Surianarayanan, V. Ranganatha, D. R. MacFarlane, and A. B. Mandal (2012). *Environ. Sci. Technol.* **46**, 4902.
- Y. Wang, L. Zhao, H. Peng, J. Wu, Z. Liu, and X. Guo (2016). *J. Chem. Eng. Data* **61**, 3266.
- A. Mohammadi and P. Veisi (2018). *J. of Environ. Chem. Eng.* **6**, 4634.
- Z. Cheng, J. Liao, B. He, F. Zhang, F. Zhang, X. Huang, and L. Zhou (2015). *ACS Sustainable Chem. Eng.* **3**, 1677.
- T. T. N. Phan, A. N. Nikoloski, P. A. Bahri, and D. Li (2019). *Appl. Surf. Sci.* **491**, 488.
- M. Wawrzekiewicz (2014). *Ind. Eng. Chem. Res.* **53**, 11838.
- B. Shi, G. Li, D. Wang, C. Feng, and H. Tang (2007). *J. Hazard. Mater.* **143**, 567.
- M. Chethana, L. G. Sorokhaibam, V. M. Bhandari, S. Raja, and V. V. Ranade (2016). *ACS Sustainable Chem. Eng.* **4**, 2495.
- S. S. Moghaddam, M. R. A. Moghaddam, and M. Arami (2010). *J. Hazard. Mater.* **175**, 651.
- D. Pathania, D. Gupta, A. H. Al-Muhtaseb, G. Sharma, A. Kumar, M. Naushad, T. Ahmad, and S. M. Alshehri (2016). *J. Photochem. Photobiol. A* **329**, 61.
- E. S. Baeissa (2016). *J. Alloys Compd.* **678**, 267.
- Z. He, C. Gao, M. Qian, Y. Shi, J. Chen, and S. Song (2014). *Ind. Eng. Chem. Res.* **53**, 3435.
- S. S. Shenvi, A. M. Isloor, A. F. Ismai, S. J. Shilton, and A. Al Ahmed (2015). *Ind. Eng. Chem. Res.* **54**, 4965.
- Z. Yang, M. Li, M. Yu, J. Huang, H. Xu, Y. Zhou, P. Song, and R. Xu (2016). *Chem. Eng. J.* **303**, 1.
- L. Malaeb and M. A. George (2011). *Desalination* **267**, 1.
- M. Arif, A. Sanger, M. Shkir, A. Shing, and R. S. Katiyar (2019). *Physica B: Condensed Matter.* **552**, 88.
- J. Xu, M. Wang, Y. Liu, J. Li, and H. Cui (2019). *Adv. Powder Technol.* **30**, 861.
- M. Alagiri, S. Ponnusamy, and C. Muthamizchelva (2012). *J. Mater. Sci. Mater. Electron.* **23**, 728.
- N. N. M. Zorkipli, N. H. M. Kausand, and A. A. Mohamad (2016). *Procedia Chem.* **19**, 626.
- A. Aslani, V. Oroojpour, and M. Fallahi (2011). *Appl. Surf. Sci.* **257**, 4056.
- M. Derakhshi, T. Jamali, M. Elyasi, M. Bijad, R. Sadeghi, A. Kamali, K. Niazazari, M. R. Shahmiri, A. Bahari, and S. Mokhtari (2013). *Int. J. Electrochem. Sci.* **8**, 8252.
- Y. Du, W. Wang, X. Li, J. Zhao, J. Ma, Y. Liu, and G. Lu (2012). *Mater. Lett.* **68**, 168.
- W. N. Wang, Y. Itoh, I. W. Lenggoro, and K. Okuyam (2004). *Mater. Sci. Eng. B* **111**, 69.
- A. G. Al-Sehemi, A. S. Al-Shihri, A. Kalam, G. Du, and T. Ahmad (2014). *J. Mol. Struct.* **1058**, 56.
- X. Song and L. Gao (2008). *J. Am. Ceram. Soc.* **91**, 3465.
- G. T. Anand, R. Nithiyavathi, R. Ramesha, S. J. Sundaram, and K. Kaviyarasu (2020). *Surf. Interface* **18**, 100460.
- J. H. Lee, J. Y. Lim, C. S. Lee, J. T. Park, and J. H. Kim (2017). *Appl. Surf. Sci.* **420**, 849.
- S. Farhadi and Z. Roostaei-Zaniyani (2011). *Polyhedron* **30**, 971.
- Z. Wei, H. Qiao, H. Yang, C. Zhang, and X. Yan (2009). *J. Alloys Compd.* **479**, 855.
- A. A. Ezhilarasi, J. J. Vijaya, K. Kaviyarasu, M. Maaza, A. Ayeshamariam, and L. J. Kennedy (2016). *J. Photochem. Photobiol. B* **164**, 352.
- F. T. Thema, E. Manikandan, A. Gurib-Fakim, and M. Maaza (2016). *J. Alloys Compd.* **657**, 655.
- A. E. Angel, J. V. Judith, K. Kaviyarasu, L. K. John, R. J. Ramalingam, and H. A. Allohedan (2018). *J. Photochem. Photobiol. B* **180**, 39–50.

37. N. Mayedwa, N. Mongwaketsi, S. Khamlich, K. Kaviyarasu, N. Matinise, M. Maaza. (2018). *App. Surf. Sci.* **446**, 266.
38. M. I. Din, A. G. Nabi, A. Rani, A. Aihetasham, and M. Mukhtar (2018). *Environ. Nanotechnol. Monit. Manage.* **9**, 29.
39. P. Kganyago, L. M. Mahlaule-Glory, M. M. Mathipa, B. Ntsendwana, N. Mketi, Z. Mbita, and N. C. Hintsho-Mbita (2018). *J. Photochem. Photobiol. B* **182**, 18.
40. A. A. Olajire and A. A. Mohammed (2020). *Adv. Powder Technol.* **31**, 211.
41. K. Lingaraju, H. R. Naika, H. Nagabhushana, K. Jayanna, S. Devaraja, and G. Nagaraju (2020). *Arab. J. Chem.* **13**, 4712.
42. M. Nasserri, F. Ahrari, and B. Zakerinasab (2016). *Appl. Organometal. Chem.* **30**, 978.
43. M. Kundu, G. Karunakaran, and D. Kuznetsov (2017). *Powder Technol.* **311**, 132.
44. R. Yuvakkumar, J. Suresh, A. Joseph Nathanael, M. Sundrarajan, and S. I. Hong (2014). *Mater. Sci. Eng. C* **41**, 17.
45. S. Z. Moghadamtousi, M. Fadaeinasab, S. Nikzad, G. Mohan, H. M. Ali, and H. A. Kadir (2015). *Int. J. Mol. Sci.* **16**, 15625.
46. A. V. Coria-Télliz, E. Montalvo-González, E. M. Yahia, and E. N. Obledo-Vázquez (2018). *Arab. J. Chem.* **11**, 662.
47. K. C. Agu and P. N. Okolie (2017). *Food Sci. Nutr.* **5**, 1029.
48. K. Karthikeyan, S. Abitha, and V. G. Saravanan Kumar (2016). *Int. J. Pharmacog. Phytochem. Res.* **8**, 1833.
49. S. Tiwari (2008). *J. Nat. Prod.* **1**, 27.
50. A. A. Adegoke, P. A. Iberi, D. A. Akinpelu, O. A. Aiyegoro, and C. I. Mboto (2010). *Int. J. Appl. Res. Nat. Prod.* **3**, 6.
51. P. Bose, S. Ghosh, S. Basak, and M. K. Naskar (2016). *J. Asian Ceram. Soc.* **4**, 1.
52. W. Wang, Y. Liu, C. Xu, C. Zheng, and G. Wang (2002). *Chem. Phys. Lett.* **362**, 119.
53. L. X. Song, Z. K. Yang, Y. Teng, J. Xia, and P. Du (2013). *J. Mater. Chem. A* **1**, 8731.
54. L. A. García-Cerda, L. E. Romo-Mendoza, and M. A. Quevedo-López (2009). *J. Mater. Sci.* **44**, 4553.
55. Y. Hanifehpour, A. Morsali, B. Mirtamizdoust, S. W. Joo, and B. Soltani (2017). *Ultrason. Sonochem.* **37**, 430.
56. J. Fang, Y. Zhang, Y. Zhou, S. Zhao, C. Zhang, M. Huang, and Y. Gao (2017). *Appl. Surf. Sci.* **412**, 616.
57. C. Yang, Y. Qing, K. An, Z. Zhang, L. Wang, and C. Liu (2017). *Mater. Chem. Phys.* **195**, 149.
58. S. Saha, M. Jana, P. Khanra, P. Samanta, H. Koo, N. C. Murmu, and T. Kuila (2015). *ACS Appl. Mater. Interfaces* **7**, 14211.
59. G. Gao, W. Gao, E. Cannuccia, J. T. Tijerina, L. Balicas, A. Mathkar, T. N. Narayanan, Z. Liu, B. K. Gupta, J. Peng, Y. Yin, A. Rubio, and P. M. Ajayan (2012). *Nano Lett.* **12**, 3518.
60. X. Song and L. Gao (2008). *J. Phys. Chem. C* **112**, 15299.
61. L. Kumari, W. Z. Li, C. H. Vannoy, R. M. Leblanc, and D. Z. Wang (2009). *Cryst. Res. Technol.* **44**, 495.
62. A. G. Al-Sehemi, A. S. Al-Shihri, A. Kalam, G. Du, and T. Ahmad (2014). *Mol. Struct.* **1058**, 56.
63. X. Li, X. Zhang, Z. Li, and Y. Qian (2006). *Solid State Commun.* **137**, 581.
64. A. T. Khalil, M. Ovais, I. Ullah, M. Ali, Z. K. Shinwari, S. Khamlich, and M. Maaza (2017). *Artif. Cells Nanomed. Biotechnol.* **12**, 1767.
65. A. K. H. Bashira, L. C. Razanamahandry, A. C. Nwanyaa, K. Kaviyarasua, W. Sabana, H. E. A. Mohamed, S. K. O. Ntwamped, F. I. Ezemaa, and M. Maazaa (2019). *J. Phys. Chem Solid* **134**, 133.
66. F. Ibrahim, M. H. Aziz, M. Fatima, F. Shaheen, S. M. Ali, and Q. Huang (2019). *Mater. Lett.* **234**, 129.
67. A. Loqman, B. El Bali, J. Lützenkirchen, P. G. Weidler, and A. Kherbeche (2017). *Appl. Water Sci.* **7**, 3649.
68. S. T. Huang, W. W. Lee, J. L. Chang, W. S. Huang, S. Y. Chou, and C. C. Chen (2014). *J. Taiwan Inst. Chem. Eng.* **45**, 1927.
69. A. Mittal, J. Mittal, A. Malviya, D. Kaur, and V. K. Gupta (2010). *J. Colloid Interface Sci.* **343**, 463.
70. K. Mohanty, J. T. Naidu, B. C. Meikap, and M. N. Biswas (2006). *Ind. Eng. Chem. Res.* **45**, 5165.
71. R. Ahmad (2009). *J. Hazard. Mater.* **171**, 767.
72. Y. H. Liao, J. X. Wang, J. S. Lin, W. H. Chung, W. Y. Lin, and C. C. Chen (2011). *Catal. Today* **174**, 148.
73. M. Mittal, M. Sharma, and O. P. Pandey (2014). *J. Nanosci. Nanotechnol.* **14**, 2725.
74. M. Sharma, T. Jain, S. Singh, and O. P. Pandey (2012). *Sol. Energy* **86**, 626.
75. V. M. Vinosel, S. Anand, M. A. Janifer, S. Pauline, S. Dhanvel, P. Praveena, and A. Stephen (2019). *J. Mater. Sci. Mater. Electron.* **30**, 9663.
76. E. A. Abdelrahman and R. M. Hegazey (2019). *J. Inorg. Organomet. Polym. Mater.* **29**, 346.
77. M. Mittal, M. Sharma, and O. P. Pandey (2014). *Sol. Energy* **110**, 386.
78. Y. Panahian, N. Arsalani, and R. Nasiri (2018). *J. Photochem. Photobiol. A* **365**, 45.
79. R. Ranjith, V. Renganathan, S. M. Chen, N. S. Selvan, and P. S. Rajam (2019). *Ceram. Int.* **45**, 12926.
80. S. Vasantharaj, S. Sathiyavimal, P. Senthilkumar, F. LewisOscar, and A. Pugazhendhi (2019). *J. Photochem. Photobiol. B* **192**, 74.

Publisher's Note Springer Nature remains neutral with regard to jurisdictional claims in published maps and institutional affiliations.